JACS
JOURNAL OF THE AMERICAN CHEMICAL SOCIETY
Communication
pubs.acs.org/JACS

Fe−P: A New Class of Electroactive Catalyst for Oxygen Reduction Reaction

Kiran Pal Singh, Eun Jin Bae, and Jong-Sung Yu*

Department of Energy Systems Engineering, Daegu Gyeongbuk Institute of Science & Technology (DGIST), Daegu 711-873, Republic of Korea

Supporting Information

ABSTRACT: It has been long thought that Fe−N−C structure, where Fe is bonded with an electronegative heteroatom N, plays a key role as nonprecious metal catalyst for oxygen reduction reaction (ORR) in fuel cells. However, electrocatalytic activity of Fe bonded with electropositive heteroatom P has never been considered for ORR. Herein we report the electrocatalytic activity for ORR of new Fe−P−C.

After Jasinski's report portraying the ability of macrocycles containing metal−nitrogen as oxygen reduction catalyst, a new era of nonprecious metal and metal-free catalyst was started.[1−3] Identifying the exact active sites for ORR is still a hot issue. However, general consensus is that the metal−N_4 bond in the macrocycle acts as an active site for the reduction of oxygen.[4−6] Keeping this in mind, various research groups have tried various compositions of carbon, nitrogen, and metal precursors.[7−10] However, these variations have not yielded any catalyst that can supersede state-of-the-art Pt catalyst in acidic medium.

Recent studies have reported that Fe and N remain adjacent to each other in electrocatalyst and that without Fe the catalyst is found to show quite low activity in acidic medium.[11] It has been predicted on the basis of molecular orbital theory that Fe atom in Fe−N/C helps develop strong back bonding with the adsorbed O_2, which causes an increase of O−O bond distance and hence facilitates ORR.[12] Until now, the exact role of N in Fe−N/C has also not been completely understood. However, various DFT and experimental observations suggest that the carbon atoms adjacent to N possess high positive spin density and atomic charge density and thus become the active catalytic sites for ORR.[13−16]

Hu et al. have reported that breaking the electroneutrality of carbon matrix is the major factor for infusing efficient ORR activity in the doped carbon.[17] Hence, even dopants with electronegativity less than that of carbon such as phosphorus or boron (P or B) are found to influence the ORR activity of the electrocatalyst in basic medium.[17−19]

Phosphorus and nitrogen belong to the same group and bear somewhat similar chemical properties. Although Fe−N/C structure has been extensively studied as an electrocatalyst, no one has ever tried to evaluate the catalytic activity of Fe−P/C structure or to enhance the catalytic property of P-doped carbon catalyst in acidic medium.

Until now, there have been several studies on transition metal phosphides, portraying the hydrogen evolution property of the catalysts.[20,21] However, the catalytic property of metal−P catalyst for ORR remains untouched. Therefore, herein for the first time, we have tried to incorporate Fe−P structure in carbon matrix and measured its activity in both acidic and basic media. It is found that catalytic activity of already active P-doped carbon in basic medium becomes more pronounced, and in acidic medium, nonactive P-doped carbon becomes active with incorporation of Fe.

Phytic acid (PA), which is considered to be principle storage form of phosphorus in plant tissues, is used as P and C source here. Ferric chloride ($FeCl_3$) is commonly used to precipitate out PA from plant samples, as PA binds with Fe irreversibly and forms insoluble complexes known as ferric phytate as shown in Scheme 1. To synthesize Fe−P bonded carbon, we have mixed

Scheme 1. Synthesis of Ferric Phytate Followed by Its Carbonization to Get Fe−P Carbon

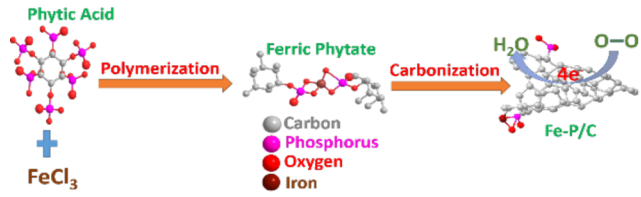

$FeCl_3$ and PA followed by their polymerization at high temperature (see experimental details in Supporting Information (SI)). The obtained polymer was then carbonized at various temperatures to obtain Fe−P-*x*, where *x* represents carbonization temperature of 800, 900, and 1000 °C. P-doped carbon (PA-900) is also prepared by carbonizing the PA polymer at 900 °C without Fe source.

Figure 1a,b shows SEM images of PA-900 and Fe−P-900, and Figure S1a,b shows SEM images of Fe-PA-800 and Fe−P-1000. Obtained P-doped carbon possesses particle-like morphology. However, on incorporation of Fe in PA carbon, the carbon starts taking sheet-like morphology, which becomes more prominent on increasing the temperature from Fe−P-800 to Fe−P-1000, portraying efficient graphitization of carbon matrix by Fe. Similarly, in TEM images of Figures 1b′ and S1a′,b′, all the catalysts prepared in the presence of Fe show sheet-like structures with porous structure in the framework.

Received: November 15, 2014
Published: February 25, 2015

DOI: 10.1021/ja511759u
J. Am. Chem. Soc. 2015, 137, 3165−3168

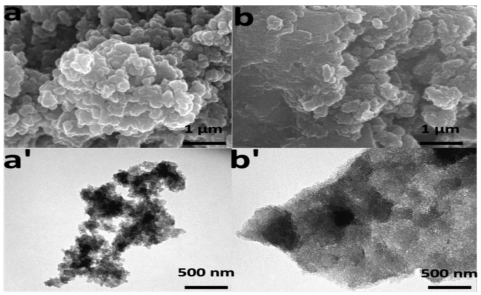

Figure 1. Typical SEM (a,b) and TEM (a′,b′) images of PA-900 and Fe−P-900, respectively.

X-ray diffraction (XRD) analysis of all the carbonized samples shows the presence of amorphous carbon as shown in Figure 2a.

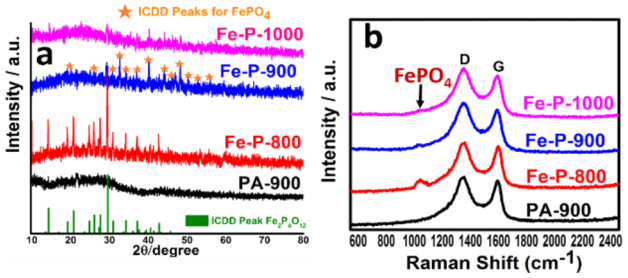

Figure 2. (a) XRD patterns and (b) Raman analysis of PA-900, Fe−P-800, Fe−P-900, and Fe−P-1000.

However, Fe−P-800 shows typical peaks of $Fe_2P_4O_{12}$, which match with ICDD card no. 01-078-2285. On increasing the carbonization temperature from 800 to 900 °C, the intensity of these peaks decreases, and new peaks for $FePO_4$ start appearing. At 1000 °C, the peaks for $Fe_2P_4O_{12}$ almost disappear, and only peaks for amorphous carbon and $FePO_4$ are found to be present.

Raman analysis was carried out to understand the crystal structure of the obtained carbon. As can be seen in Figure 2b, all the samples showed typical D and G bands, designated to disordered and graphitic phases in carbon, respectively. However, appearance of a new band at ∼1050 cm^{-1} is seen in Fe−P samples. This peak arises due to symmetric PO_4^{3-} stretching mode associated with the PO_4^{3-} tetrahedral and can be ascribed to the presence of $FePO_4$.[22] High intensity of this peak in Fe−P-800 indicates the overlapping of peaks originating from both $FePO_4$ and $Fe_2P_4O_{12}$ phases in high amount in the sample. On increasing the temperature, the peak intensity keeps on decreasing mainly due to decomposition of $Fe_2P_4O_{12}$, proclaiming less stability of the species at higher temperature.

The chemical composition of the prepared catalysts was further evaluated using X-ray photoelectron spectroscopy (XPS) analysis. Figure S2 shows the peak survey of PA-900, Fe−P-800, Fe−P-900, and Fe−P-1000 samples. As can be seen in Table 1, with introduction of Fe in PA, the P doping level increases from 2.9 for PA-900 to 3.1 for Fe−P-900, indicating interaction between P and Fe. However, a decreasing trend in P doping level is observed with increasing temperature, from 3.4 for Fe−P-800 to 3.1 for Fe−P-900 and 2.3 for Fe−P-1000. Furthermore, Fe content also decreases on increasing temperature as shown in Figure 3a, which can be in part due to the formation of carbon layer around Fe particle at higher temperature, hence making the XPS electron beam impermeable to reach and analyze Fe.[23] XPS Fe 2p core level spectra shows Fe $2p_{3/2}$ peak centered around

Table 1. Atomic Composition of Catalysts Obtained from XPS and EDS Spectra

	atomic composition (%) (XPS/EDS)			
sample name	C	O	P	Fe
PA-900	83.5	13.6	2.9	
Fe−P-800	82.7/77.9	12.9/14.6	3.4/4.9	1.0/2.6
Fe−P-900	84.9/80.5	11.5/12.9	3.1/4.5	0.5/2.1
Fe−P-1000	87.9/83.4	9.5/11.1	2.3/3.9	0.3/1.6
Fe−P-900 (AT)	83.8/77.9	13.1/16.4	2.7/3.8	0.4/1.9

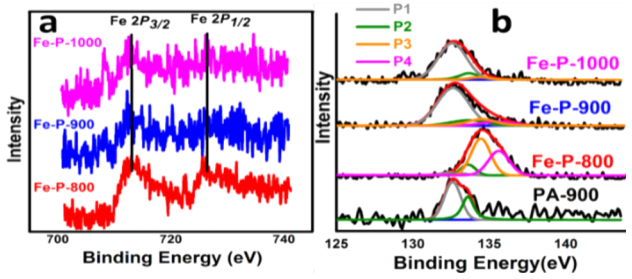

Figure 3. (a) Fe 2p narrow scan spectra and (b) deconvolution profiles of P 2p spectra of as-prepared catalysts.

711.1 eV and shows the presence of Fe in metallic Fe, Fe(II), or Fe(III) state. XPS peak at 725 eV corresponding to Fe $2p_{1/2}$ level of Fe species is also found decreasing with increasing temperature. Energy dispersive spectroscopy (EDS) analysis may provide a more realistic picture of Fe content (Figure S3), also indicating the decrease of Fe, but much less of a decrease on increasing the temperature as summarized in Table 1 as well.

The XPS spectra of phosphorus is deconvoluted into four major components, P1 (132.5 eV) assigned to P−C, P2 (133.6 eV) assigned to P−O, P3 (134.2 eV) assigned to P−O−Fe, and P4 (135.5 eV) assigned to metaphosphate, an oxyanion having empirical formula PO_3^-.[24] In Fe-free PA-900, two peaks for P−C (P1) and P−O (P2) can be seen, showing that a major part of phosphorus is doped in carbon, and the remaining is present in the oxidized form. However, with the addition of Fe in PA, a significant shift in phosphorus binding energy has been noticed for Fe−P-800, which can be ascribed to the formation of HPO_4^{2-} ion due to hydration of phosphates.[25] Furthermore, for Fe−P-800, most of P is found to be present in the form of P−O−Fe entity (P3),[26] and the rest is present in the oxidized forms (P2 and P4). Only a very small portion is doped in carbon matrix (P1) at this relatively low temperature as shown in Figure 3b. On increasing the temperature for Fe−P-900 and Fe−P-1000, the increase in P1 and significant reduction in P3 and P4 are observed, signifying that at higher temperature, Fe is mainly used to help P get doped into carbon and to catalyze the graphitization of carbon along with less involvement to phosphate formation as shown in Table S1. This reduction in Fe-phosphate amount is also visible in Raman and XRD data.

To further analyze the surface textural properties of the catalysts, Brunauer−Emmett−Teller specific surface area was characterized by nitrogen isothermal adsorption/desorption measurements (Figure S4). It can be seen that PA-900 possesses high BET surface area of 577 m^2/g. Such a high surface area without use of any template can be ascribed to the pore-generating ability of phosphorus acidic groups attached to PA.[27] Interestingly, with the introduction of Fe in PA, a huge upsurge in surface area is observed mainly from an increase in micropores (Table S2). Fe−P-800 shows surface area of 1068 m^2/g, whereas

DOI: 10.1021/ja511759u
J. Am. Chem. Soc. 2015, 137, 3165−3168

the surface areas of Fe−P-900 and Fe−P-1000 are found to be 1371 and 1659 m^2/g, respectively.

The electrocatalytic activity of all the prepared catalysts was studied using rotating ring disk electrode (RRDE) technique in 0.1 M $HClO_4$/0.1 M KOH at a rotation speed of 1600 rpm with a scan rate of 10 mV/s (Figures 4 and S6). A clear advantage in

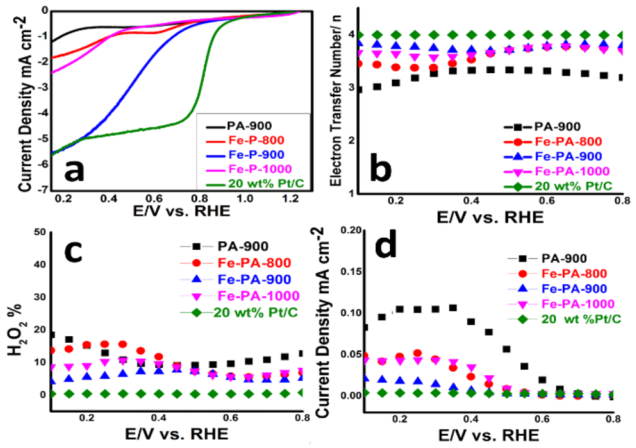

Figure 4. Electrochemical activity studied using RRDE technique at 1600 rpm in O_2-saturated 0.1 M $HClO_4$ solution. (a) Effect of carbonization temperature on LSV curves, (b) electron number transferred per oxygen molecule, (c) $\%HO_2^-$ production, and (d) current density on ring electrode during ORR reaction for PA-900, Fe−P-*x*, and 20% Pt/C (E-TEK).

terms of both ORR onset potential and limiting current is observed on incorporating Fe in PA. Figure 4a shows a linear sweep voltammogram (LSV) of all the catalysts in acidic medium. Interestingly, an almost inactive P-doped carbon (PA-900) with onset potential 0.31 V becomes highly active with Fe incorporation (Fe−P-900) showing high onset potential at 0.84 V. Varying onset potentials have been observed on varying the carbonization temperature. It can be noticed that at low temperature Fe−P-800 reveals low ORR activity with 0.48 V onset potential (the hump at ∼0.79 V vs RHE in O_2 is not due to the ORR process, but might be due to the adsorption/desorption of surface oxygen or hydrogen or due to the double layer charging, as can be seen from the LSV curve of Fe−P-800 in N_2-saturated electrolyte in Figure S7e), which might be due to low doping of P in carbon matrix as can be seen from the P deconvolution for Fe−P-800 and Table S1. Similarly, in Fe−P-1000, even though the amount of P doped into carbon is high along with high surface area, the amount of active Fe−P is very low, which may cause reduction in its ORR activity with onset potential 0.51 V. This result may signify that both P−C and Fe−P species synergistically play a significant role in enhancing the ORR activity and high activity of Fe−P species in ORR can be realized only in the condition of the efficient doping of P in carbon matrix.

Figure 4b shows the electron number transferred for each catalyst including Pt/C. Following the excellent kinetics of Pt (4.0 electron transfer no.) in acid medium for ORR, Fe−P-900 shows electron transfer number of 3.8 very close to that of Pt/C, whereas the Fe-free counterpart PA-900 shows the value of 2.9, which is much lower than that of Fe−P-900. Similar to the LSV results, ORR kinetics also decreases on varying the carbonization temperature for Fe−P-800 (3.5) and Fe−P-1000 (3.6). Figure 4c,d shows the percentage formation of H_2O_2 and current obtained at the ring electrode due to H_2O_2 reduction, respectively. As can be seen here also, Fe−P-900 outperforms all the other prepared catalysts. The % H_2O_2 formation of Fe−P-900 is 4.13%, which is a bit higher than 0.37% for Pt/C. However, the value is much better than 18.8% for Fe-free PA-900, 13.3% for Fe−P-800, and 8.4% for Fe−P-1000. These results clearly display the superiority of Fe−P-900 over Fe-free PA-900, indicating the possibility of new Fe−P functionalized carbon electrocatalyst.

Furthermore, the mass activity of the catalysts was estimated by extrapolating the kinetically controlled Tafel slope in Figure S5a. The Fe−P-900 shows mass activity of 0.018 A/mg vs RHE, which is still lower than Pt/C catalyst with 0.054 A/mg at 0.9 V vs RHE in acidic medium. However, the mass activity of Fe−P-900 is far better than PA-900 (0.0009 A/mg), Fe−P-800 (0.0027 A/mg), and Fe−P-1000 (0.0042 A/mg). Moreover, the Tafel slope for Fe−P-900 is also quite smaller in comparison to the other prepared catalysts, which clearly shows the adsorption of O_2 is high and facile on Fe−P-900.

We also measured the ORR in alkaline medium vs RHE (0.1 M KOH) using RRDE as shown in Figure S6a. The onset potential and limiting current of Fe−P-900 increase drastically (0.95 V and 5.01 mA/cm^2) as compared to those of PA-900 (0.75 V and 2.5 mA/cm^2), but are a little less than Pt/C (0.97 V and 5.1 mA/cm^2). Variation in ORR activity similar to that in acidic conditions is observed in basic conditions as well. Fe−P-800 shows onset potential (0.81 V and 3.01 mA/cm^2), better than PA-900. However, on increasing the temperature, onset potential first improves (Fe−P-900) and then decreases (Fe−P-1000) (0.87 V and 4.6 mA/cm^2). It shows that catalytic activity of Fe−P catalysts in basic condition also depends on the presence of both Fe−P and P−C species. Furthermore, the Fe−P-900 catalyst in alkaline medium shows almost similar kinetics to various well-known Fe−N catalysts as can be seen in Table S4.[28−33] Figure S6b shows the electron number transferred in all the prepared catalysts during ORR. PA-900 due to the absence of Fe is found to portray very weak kinetics with electron transfer number of ∼2.9. However, Fe−P-900 shows a number of 3.62, a little bit lesser than (3.9) the state-of-the-art Pt/C catalyst, whereas for Fe−P-800 and Fe−P-1000, the number is found to be 3.28 and 3.41, respectively. Similarly, as can be seen from Figure S6c, the H_2O_2 production for Fe−P-900 (1.3%) catalyst is more or less similar to Pt/C (1.1%) in applied potential range, while PA-900, Fe−P-800, and Fe−P-1000 catalysts show high H_2O_2 production with 17.16, 11.90, and 8.26%, respectively. Because of Fe addition, a reduction in ring current for Fe−P-900 (0.12 mA/cm^2) is also observed as compared to PA-900 (0.53 $mA\ cm^{-2}$) in Figure S6d. The ring current of Fe−P-800 (0.40 mA/cm^2) and Fe−P-1000 (0.23 mA/cm^2) was also less than PA-900, proving the important role of both Fe−P and P−C in the preparation of an efficient ORR catalyst.

Figure S7a,b shows the cyclic voltammogram (CV) of all the catalysts in acidic and alkaline media. In alkaline conditions, a well-defined ORR peak was observed for both PA-900 and Fe−P-900. Interestingly, Fe−P-900 reveals the ORR peak at more positive potential than Fe-free PA-900, Fe−P-800, and Fe−P-1000. The area under the CV curve is also very pronounced for Fe−P-900, showing the increased ORR active sites. These studies thus clearly show that well-prepared Fe−P can be promising for ORR in the present form as it displays superior ORR kinetics in both acidic and alkaline conditions.

The *J*−*T* response of the Fe−P-900 catalyst over repeated cycles for ∼7 h is shown in Figure S8a. It can be seen that Fe−P-900 catalyst retains almost 81% of its initial current after cycling,

DOI: 10.1021/ja511759u
J. Am. Chem. Soc. 2015, 137, 3165−3168

which is almost similar to various Fe−N doped catalysts.[19,29,30] However, only ∼69% of the initial current is seen in the state-of-the-art Pt/C catalyst. This superior stability of the catalyst can be ascribe to the higher stability of active P−C and Fe−P in the catalyst. As can be seen from Table S3, a significant portion of the active P−C and Fe−P contents still remains even after the repeated cycles despite some decrease. However, the loss in activity can be attributed mainly to the corrosion of carbon surface and leaching-out of some P and Fe from the carbon matrix, which causes an increase in the charge transfer resistance in Fe−P-900 catalyst after cycling test (Figure S8b). The morphology and chemical composition of the catalyst retrieved after the cycling test are shown in Figures S9a,b and S10. Fe−P-900 sample after the cycling test is broken into interconnected particle-like morphology from its original sheet-like one. Furthermore, XPS analysis also shows the reduction in carbon, Fe, and P percentage and increase in oxygen percentage (Table 1) after the cycling test.

In conclusion, we have synthesized a new class of metal−heteroatom-bonded carbon (Fe−P) catalysts and measured their electrocatalytic activity toward ORR in both acidic and alkaline media. It is found that with the addition of Fe in phytic acid followed by carbonization, a new species Fe−P is introduced into the carbon matrix, which is highly susceptible to the carbonization temperature. With the introduction of Fe−P species, the ORR activity of the prepared Fe−P-900 sample improves significantly in both acidic and alkaline media compared to nonactivity of Fe-free PA-900 in acidic medium. In addition to improved catalytic activity, improvement in catalytic kinetics was also observed, showing that Fe−P-900 follows ∼4 electron pathway in both acidic and alkaline media for ORR. From the various studies carried out in the present work, it becomes evident that the ORR activity in such a class of catalyst that depends highly on the presence of both Fe−P species and P−C bond, and absence of any one of these species significantly deteriorates the catalytic activity. Current study on catalytic activity of Fe−P, where Fe is bonded with an electropositive P species instead of electronegative N, can definitely open up new dimensions toward understanding the role of Fe in ORR. Furthermore, as strong synergistic interactions between N and P were observed for multiple-doped carbon materials in earlier work,[24] we think that, with the combination of both N and P elements, a much more efficient catalyst can be developed in upcoming research. Such cost-effective efficient nonprecious metal−heteroatom carbon catalysts will be a promising replacement to costly Pt-based electrocatalysts in fuel cells.

■ ASSOCIATED CONTENT

Supporting Information

Experimental procedures and characterization data. This material is available free of charge via the Internet at http://pubs.acs.org.

■ AUTHOR INFORMATION

Corresponding Author

*jsy119@gmail.com

Notes

The authors declare no competing financial interest.

■ ACKNOWLEDGMENTS

This work was supported by NRF grant (NRF-2010-0029245) and Global Frontier R&D Program on Center for Multiscale Energy System (NRF-2011-0031571) funded by the Ministry of Education, Science and Technology. Authors also would like to thank KBSI at Jeonju, Daejeon, and Chuncheon for SEM, TEM, and XPS measurements.

■ REFERENCES

(1) Wu, G.; More, K. L.; Johnston, C. M.; Zelenay, P. *Science* **2011**, *332*, 443.
(2) Gong, K.; Du, F.; Xia, Z.; Durstock, M.; Dai, L. *Science* **2009**, *323*, 760.
(3) Singh, K. P.; Song, M. Y.; Yu, J.-S. *J. Mater. Chem. A* **2014**, *2*, 18115.
(4) Lefevre, M.; Dodelet, J. P. *J. Phys. Chem. B* **2000**, *104*, 11238.
(5) Li, W.; Wu, J.; Higgins, D. C.; Choi, J.-Y.; Chen, Z. *ACS Catal.* **2012**, *2*, 2761.
(6) Kattel, S.; Wang, G. *J. Mater. Chem. A* **2013**, *1*, 10790.
(7) Oh, H.-S.; Oh, J.-G. B.; Roh, I.; Hwang; Kim, H. *Electrochem. Commun.* **2011**, *13*, 879.
(8) Bezerra, C. W. B.; Zhang, L.; Lee, K.; Liu, H.; Marques, A. L. B.; Marques, E. P.; Wang, H.; Zhang, J. *Electrochim. Acta* **2008**, *53*, 4937.
(9) Jahan, M.; Bao, Q.; Loh, K. P. *J. Am. Chem. Soc.* **2012**, *134*, 6707.
(10) Unni, S. M.; Illathvalappil, R.; Gangadharan, P. K.; Bhangea, S. N.; Kurungot, S. *Chem. Commun.* **2014**, *50*, 13769.
(11) Li, Y. G.; Zhou, W.; Wang, H. L.; Xie, L. M.; Liang, Y. Y.; Wei, F.; Idrobo, J. C.; Pennycook, S. J.; Dai, H. J. *Nat. Nanotechnol.* **2012**, *7*, 394.
(12) Alt, H.; Binder, H.; Sandstede, G. *J. Catal.* **1973**, *28*, 8.
(13) Zhang, L. P.; Xia, Z. H. *J. Phys. Chem. C* **2011**, *115*, 11170.
(14) Li, H.; Li, Y.; Koper, M. T. M.; Calle-Vallejo, F. *J. Am. Chem. Soc.* **2014**, *136*, 15694.
(15) Negro, E.; Vezzù, K.; Bertasi, F.; Schiavuta, P.; Toniolo, L.; Polizzi, S.; Noto, V. D. *ChemElectroChem* **2014**, *1*, 1359.
(16) Negro, E.; Polizzi, S.; Vezzù, K.; Toniolo, L.; Cavinato, G.; Noto, V. D.; Int, J. *Hydrogen Energy* **2014**, *39*, 2828.
(17) Yang, L.; Jiang, S.; Zhao, Y.; Zhu, L.; Chen, S.; Wang, X.; Wu, Q.; Ma, J.; Ma, Y.; Hu, Z. *Angew. Chem., Int. Ed.* **2011**, *50*, 7132.
(18) Liu, Z.-W.; Peng, F.; Wang, H.-J.; Yu, H.; Zheng, W.-X.; Yang, J. *Angew. Chem.* **2011**, *123*, 3315.
(19) Yang, D. S.; Bhattacharjya, D.; Inamdar, S.; Park, J.; Yu, J.-S. *J. Am. Chem. Soc.* **2012**, *134*, 16127.
(20) Liu, Q.; Tian, J.; Cui, W.; Jiang, P.; Cheng, N.; Asiri, A. M.; Sun, X. *Angew. Chem., Int. Ed.* **2014**, *53*, 6710.
(21) Xu, Y.; Wu, R.; Zhang, J. F.; Shi, Y. M.; Zhang, B. *Chem. Commun.* **2013**, *49*, 6656.
(22) Pasternak, M. P.; Rozenberg, G. K.; Milner, A. P.; Amanowicz, M.; Zhou, T.; Schwarz, U.; Syassen, K.; Miller, R. D.; Hanfland, M.; Brister, K. *Phys. Rev. Lett.* **1997**, *79*, 4409.
(23) Choi, C. H.; Chung, M. W.; Park, S. H.; Woo, S. I. *Phys. Chem. Chem. Phys.* **2013**, *15*, 1802.
(24) Razmjooei, F.; Singh, K. P.; Song, M. Y.; Yu, J.-S. *Carbon* **2014**, *78*, 257−267.
(25) Yu, D.; Wu, C.; Kong, Y.; Xue, N.; Guo, X.; Ding, W. *J. Phys. Chem. C* **2007**, *111*, 14394.
(26) Daou, T. J.; Colin, S. B.; Greneche, J. M.; Thomas, F.; Derory, A.; Bernhardt, P.; Legare, P.; Pourroy, G. *Chem. Mater.* **2007**, *19*, 4494.
(27) Nahil, M. A.; Williams, P. T. *Biomass Bioenergy* **2012**, *37*, 142.
(28) Yan, X. H.; Xu, B. Q. *J. Mater. Chem. A* **2014**, *2*, 8617.
(29) Wu, Z. S.; Yang, S.; Sun, Y.; Parvez, K.; Feng, X.; Müllen, K. *J. Am. Chem. Soc.* **2012**, *134*, 9082.
(30) Jiang, Y.; Lu, Y.; Lv, X.; Han, D.; Zhang, Q.; Niu, L.; Chen, W. *ACS Catal.* **2013**, *3*, 1263.
(31) Cheon, J. Y.; Kim, T.; Choi, Y. M.; Jeong, H. Y.; Kim, M. G.; Sa, Y. J.; Kim, J.; Lee, Z.; Yang, T. H.; Kwon, K.; Terasaki, O.; Park, G. G.; Adzic, R. R.; Joo, S. H. *Sci. Rep.* **2013**, *3*, 2715.
(32) Liang, J.; Zheng, Y.; Chen, J.; Liu, J.; Hulicova-Jurcakova, D.; Jaroniec, M.; Qiao, S. Z. *Angew. Chem., Int. Ed.* **2012**, *51*, 3892.
(33) Yang, D.-S.; Song, M. Y.; Singh, K. P.; Yu, J.-S. *Chem. Commun.* **2015**, *51*, 2450.

DOI: 10.1021/ja511759u
J. Am. Chem. Soc. 2015, 137, 3165−3168